Research Square

Preprints are preliminary reports that have not undergone peer review.
They should not be considered conclusive, used to inform clinical practice,
or referenced by the media as validated information.

Symmetry-resolved Raman fingerprints of uniaxial and biaxial strain in WSe 2

Mariana M. Gomes
Universidad Autónoma de Madrid
Pablo Ares
Universidad Autónoma de Madrid
Andres Castellanos-Gomez
Consejo Superior de Investigaciones Científicas
Carmen Munuera
Consejo Superior de Investigaciones Científicas
Álvaro Rodríguez
alvaro.rodriguezr@uam.es

Universidad Autónoma de Madrid

Article

Keywords:

Posted Date: November 25th, 2026

DOI: https://doi.org/10.21203/rs.3.rs-10293900/v1

License: This work is licensed under a Creative Commons Attribution 4.0 International License.
Read Full License

Additional Declarations: No competing interests reported.

Symmetry-resolved Raman fingerprints of uniaxial and biaxial strain in WSe_2

Mariana M. Gomes[1,2*], Pablo Ares[1,2,3], Andres Castellanos-Gomez[4], Carmen Munuera[4], Álvaro Rodríguez[1,2,4 *]

[1]Departamento de Física de la Materia Condensada, Universidad Autónoma de Madrid, Madrid, 28049, Spain.

[2]Condensed Matter Physics Center (IFIMAC), Universidad Autónoma de Madrid, Madrid, 28049, Spain.

[3]Instituto Nicolás Cabrera (INC), Universidad Autónoma de Madrid, Madrid, 28049, Spain.

[4]2D Foundry group, Instituto de Ciencia de Materiales de Madrid (ICMM-CSIC), C. Sor Juana Inés de la Cruz, 3, Madrid, 28049, Spain.

*Corresponding author(s): alvaro.rodriguezr@uam.es, mariana.mgomes@uam.es

Abstract

Raman shifts in two-dimensional materials are widely used to probe mechanical strain. In WSe_2, however, the spectral overlap between the in-plane E and out-of-plane A_1 phonon modes complicates the identification of strain symmetry, particularly when the strain-induced splitting of the in-plane mode is not fully resolved and conventional Raman measurements can produce ambiguous spectral evolution. Here, we demonstrate that polarization-resolved Raman spectroscopy provides direct symmetry-specific fingerprints to distinguish uniaxial and biaxial strain in WSe_2. While both strain regimes can generate similar apparent Raman peak splitting in unpolarized Raman spectra, their polarization responses reveal fundamentally different symmetry fingerprints. Under uniaxial strain, symmetry lowering lifts the degeneracy of the in-plane phonon mode and produces a strongly anisotropic Raman response under sample rotation. In contrast, biaxial strain preserves the symmetry and maintains an angularly invariant Raman response despite the emergence of similar spectral separations. These results establish polarization-resolved Raman spectroscopy as a robust experimental approach for identifying strain symmetry and, more broadly, for distinguishing strain-induced spectral evolution arising from fundamentally different physical mechanisms in two-dimensional materials with overlapping Raman modes.

Introduction

Strain engineering is a common strategy for tuning the optical, vibrational, and electronic properties of two-dimensional semiconductors.[1–3] In transition metal dichalcogenides (TMDCs), the reduced dimensionality and strong coupling between lattice and electronic degrees of freedom make the phonon response particularly sensitive to mechanical deformation.[4,5] As a consequence, Raman spectroscopy has become one of the most widely used techniques to probe strain through phonon frequency shifts, linewidth variations, and mode splitting, together with complementary optical probes such as reflectance and photoluminescence spectroscopy.[6–9] Previous studies have shown that uniaxial strain lowers the crystal symmetry, lifts the degeneracy of the in-plane phonon mode, and modifies the Raman selection rules, giving rise to characteristic polarization-dependent Raman responses.[10,11]

Among TMDCs, WSe_2 presents a particularly challenging case from a spectroscopic perspective. In monolayer and few-layer WSe_2,[12] the in-plane E and out-of-plane A_1 phonons lie within a narrow spectral window around ~250 cm^{-1}, often resulting in partially unresolved Raman features whose relative intensity strongly depends on excitation wavelength, layer number, and resonance conditions.[13–17] The spectrum is further complicated by nearby first- and second-order Raman modes, particularly the resonant 2LA(M) mode, which overlaps the E/A_1 spectral region, further increasing spectral congestion.[13,14,18,19] Consequently, interpreting the Raman response of WSe_2 under mechanical deformation is considerably more challenging than in other TMDCs, where the relevant phonon modes are spectrally well separated.

Previous studies have reported strain-induced spectral splitting and mode-dependent phonon shifts in WSe_2 and related TMDCs.[15,20,21] However, similar Raman spectra can originate from fundamentally different strain symmetries (Supplementary Note 1). Under uniaxial strain, symmetry lowering lifts the degeneracy of the in-plane E phonon mode, whereas biaxial strain preserves the lattice symmetry and instead produces different shift rates of the overlapping E and A_1 modes.[22–24] Consequently, the appearance of two Raman peaks within the E/A_1 spectral region is frequently interpreted as evidence of in-plane mode

splitting, although it may arise from fundamentally different physical mechanisms. Conventional unpolarized Raman spectroscopy alone is therefore often insufficient to determine the underlying strain symmetry. In this context, the key question is not simply how the Raman spectrum evolves under strain, but whether the underlying lattice symmetry is preserved or broken under deformation. This ambiguity complicates the reliable identification of the strain symmetry from conventional Raman spectra.

Polarization-resolved Raman spectroscopy provides direct experimental access to this symmetry information because strain-induced symmetry changes modify the Raman tensors and selection rules, thereby altering the angular and polarization dependence of the Raman response.[25,26] Recent theoretical and experimental studies have demonstrated the sensitivity of polarization-dependent Raman spectroscopy to crystal symmetry, strain-induced anisotropy, and local lattice distortions in TMDCs and related low-dimensional materials.[27–31] For instance, in MoS_2, both theoretical and experimental studies have shown that uniaxial strain lifts the degeneracy of in-plane phonon modes and modifies their polarization dependence, enabling the determination of the strain magnitude and even crystallographic orientation.[10,11] In highly anisotropic black phosphorus, angle-resolved Raman measurements under uniaxial strain have likewise revealed a strong dependence of the phonon response on the strain direction.[32] Another example is polarization-dependent Raman spectroscopy of highly strained hexagonal boron nitride (hBN) bubbles, which enabled the extraction of shear deformation potential from strain-induced phonon splitting.[33] These studies demonstrate that polarization-resolved Raman spectroscopy can provide information not only on the magnitude of strain, but also on its direction, anisotropy, and symmetry. In this context, polarization-resolved Raman spectroscopy provides a particularly valuable approach for investigating strain in WSe_2, where the lifting of phonon degeneracies and the associated changes in Raman selection rules can be used to probe the symmetry of the strained state. Nevertheless, direct experimental fingerprints for unambiguously distinguishing uniaxial and biaxial strain in WSe_2 have not been clearly established, largely because of the spectral congestion of the E/A_1 spectral region, its strong excitation dependence, and the limited availability of homogeneous large-strain platforms.

The challenge is therefore not to detect strain itself, but to determine the symmetry of the applied deformation from the Raman response. This requires observables that directly probe lattice symmetry rather than relying solely on spectral shifts.

A second experimental challenge is achieving sufficiently large deformation while maintaining reliable optical access to the strained region.[34] Recent advances in strain-transfer engineering have substantially improved the attainable strain in atomically thin semiconductors. In particular, gold-assisted exfoliation provides strong interfacial coupling between TMDCs and Au substrates, leading to efficient strain transfer and enabling access to large, spatially homogeneous uniaxial and biaxial strain. Previous studies employing this approach demonstrated enhanced strain transfer together with large strain-induced optical modulation in TMDCs.[35,36]

Here, we combine large-strain engineering with polarization-resolved Raman spectroscopy to directly probe the symmetry-dependent vibrational response of WSe_2 under uniaxial and biaxial deformation. We show that strain geometries producing similar conventional Raman spectra exhibit fundamentally different polarization signatures, providing direct experimental fingerprints of the underlying strain symmetry. Uniaxial strain lowers the lattice symmetry, leading to anisotropic Raman tensors, activation of the out-of-plane mode under crossed polarization, and lifting of the in-plane mode degeneracy. In contrast, biaxial strain preserves the lattice symmetry and maintains an isotropic polarization response despite the progressive spectral separation of the overlapping phonon modes. These results establish polarization-resolved Raman spectroscopy as a robust and experimentally accessible strategy for identifying strain symmetry in WSe_2 and, more broadly, in two-dimensional semiconductors where complex strain fields coexist.

Results and Discussion

Excitation-dependent Raman response of WSe_2 under uniaxial strain

Samples were prepared by gold-assisted exfoliation,[37,38] which enables improved strain transfer in atomically thin TMDCs. The uniaxial and biaxial strain platforms used in this

work were adapted from our previous studies on strain engineering in TMDCs.[39–41] Further details regarding the samples and setups are provided in Supplementary Note 1.

We first investigate the Raman response of WSe_2 under uniaxial strain using 532 nm excitation (Figure 1a). Trilayer WSe_2 was selected because it combines access to larger strain values with stronger Raman intensity, resulting in improved spectral contrast. At zero strain, the spectra are dominated by a broad Raman feature centered around 250 cm^{-1}, commonly assigned to overlapping in-plane E and out-of-plane A_1 modes, together with a weaker resonant 2LA(M) mode near 260 cm^{-1}. Throughout this work, the E and A_1 notation follows the C_{3v} symmetry of WSe_2 on Au substrates.[42] Under uniaxial strain, the symmetry is reduced from C_{3v} to C_1, and the Raman-active modes become non-degenerate A-type modes. A detailed discussion of the mode assignment, symmetry notation, and corresponding Raman selection rules is provided in Supplementary Note 2.

Upon increasing strain, a second peak progressively emerges on the low-frequency side of the broad E/A_1 spectral region, eventually leading to a well-defined double-peak structure at higher strains. This behavior is consistent with the strain-induced splitting of the in-plane mode previously reported in MoS_2 under uniaxial strain.[10,43,44] At lower strain, however, the spectra remain dominated by the intense and relatively broad contribution around the A_1 spectral region, making the strain-induced evolution difficult to resolve unambiguously.

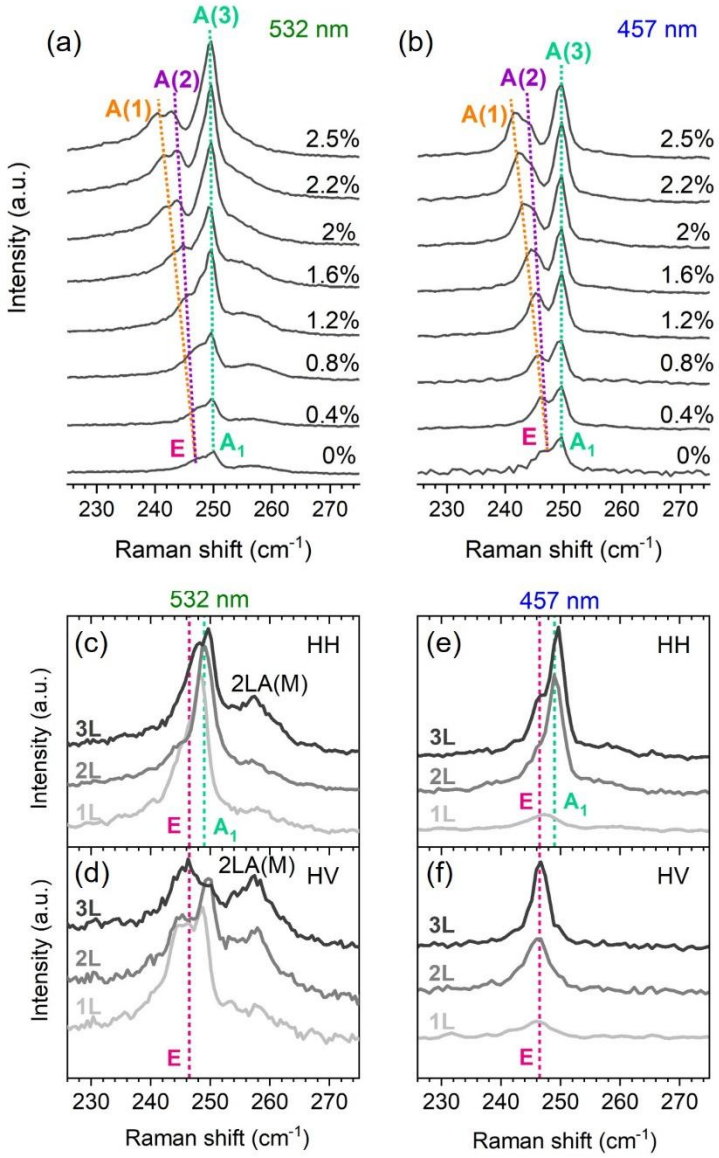

Figure 1. Excitation-dependent Raman response of WSe_2 under uniaxial strain. (a) Unpolarized Raman spectra of 3L WSe_2 acquired under increasing uniaxial strain using (a) 532 nm and (b) 457 nm excitations. (c,d) Parallel (HH) and crossed (HV) polarized Raman spectra of unstrained 1L–3L WSe_2 acquired using 532 nm excitation. (e,f) Parallel (HH) and crossed (HV) polarized Raman spectra acquired using 457 nm excitation. Dotted lines are used as guides to the eye to better visualize the position of the Raman modes. Pink and green lines indicate the in-plane (E) and out-of-plane (A1) modes, respectively. Due to the reduced symmetry induced by uniaxial strain, the in-plane E mode splits into two components, A(1) (orange line) and A(2) (purple line), and the out-of-plane A1 becomes A(3).

Figures 1c and 1d compare the polarization-resolved Raman spectra of unstrained 1L–3L WSe_2 acquired using 532 nm excitation under parallel (HH) and crossed (HV) configurations. While the HH spectra exhibit the expected layer-dependent evolution, a pronounced residual

Raman contribution remains active within the A_1 spectral region under HV polarization. Since the out-of-plane A_1 mode is expected to be inactive in the crossed-polarization geometry for the preserved lattice symmetry,[45] this residual intensity indicates the presence of additional Raman contribution that overlaps with the A_1 mode position under 532 nm excitation but not under 457 nm excitation. This pronounced excitation-energy dependence indicates this effect is likely associated with resonant or overlapping multiphonon contributions. This Raman contribution has not been reported on freestanding WSe_2 layers under 532 nm excitation [19], therefore Au contribution cannot be entirely excluded.

To determine whether the additional contribution observed at 532 nm originates from resonance effects, the same measurements were repeated using 457 nm excitation. Figures 1e–f show the corresponding Raman spectra recorded using 457 nm excitation. Compared with 532 nm excitation, these spectra exhibit a considerably cleaner response within the E/A_1 spectral region. The residual contribution observed under crossed polarization is strongly suppressed, while the resonant 2LA(M) mode becomes nearly negligible. As a result, the individual E and A_1 contributions become significantly better resolved. The improved spectral definition enables a more reliable analysis of the symmetry evolution under strain (Figure 1b). The progressive separation of the E and A_1 contributions gives rise to a well-defined double-peak structure, whereas the genuine splitting of the in-plane mode becomes directly observable only at strain values above ~1.6%. The fitted phonon modes frequencies and the in-plane splitting as functions of strain, including the corresponding shift rates are presented in Supplementary Note 5. Similar evolution is observed for both mono and bilayer WSe_2 on Au (Supplementary Note 3). Therefore, the following analysis focuses on trilayer WSe_2, whose higher Raman intensity provides superior spectral contrast and more closely reflects the intrinsic response of WSe_2 while still allowing efficient strain transfer. The cleaner polarization response obtained at 457 nm therefore forms the basis for the symmetry analysis presented in the following sections.

Polarization-resolved Raman fingerprints of uniaxial strain

To probe the symmetry evolution induced by uniaxial strain of 1.6%, polarization-resolved Raman measurements were performed under parallel (HH) and crossed (HV) configurations.

The angular dependence was obtained by rotating the sample together with the straining setup, thereby maintaining the applied strain while keeping the polarizer/analyzer configuration fixed. In contrast, in Ref. [46], the straining setup remains fixed and the sample is reoriented to apply strain along different crystallographic directions, requiring the strain to be released and reapplied for each sample orientation.

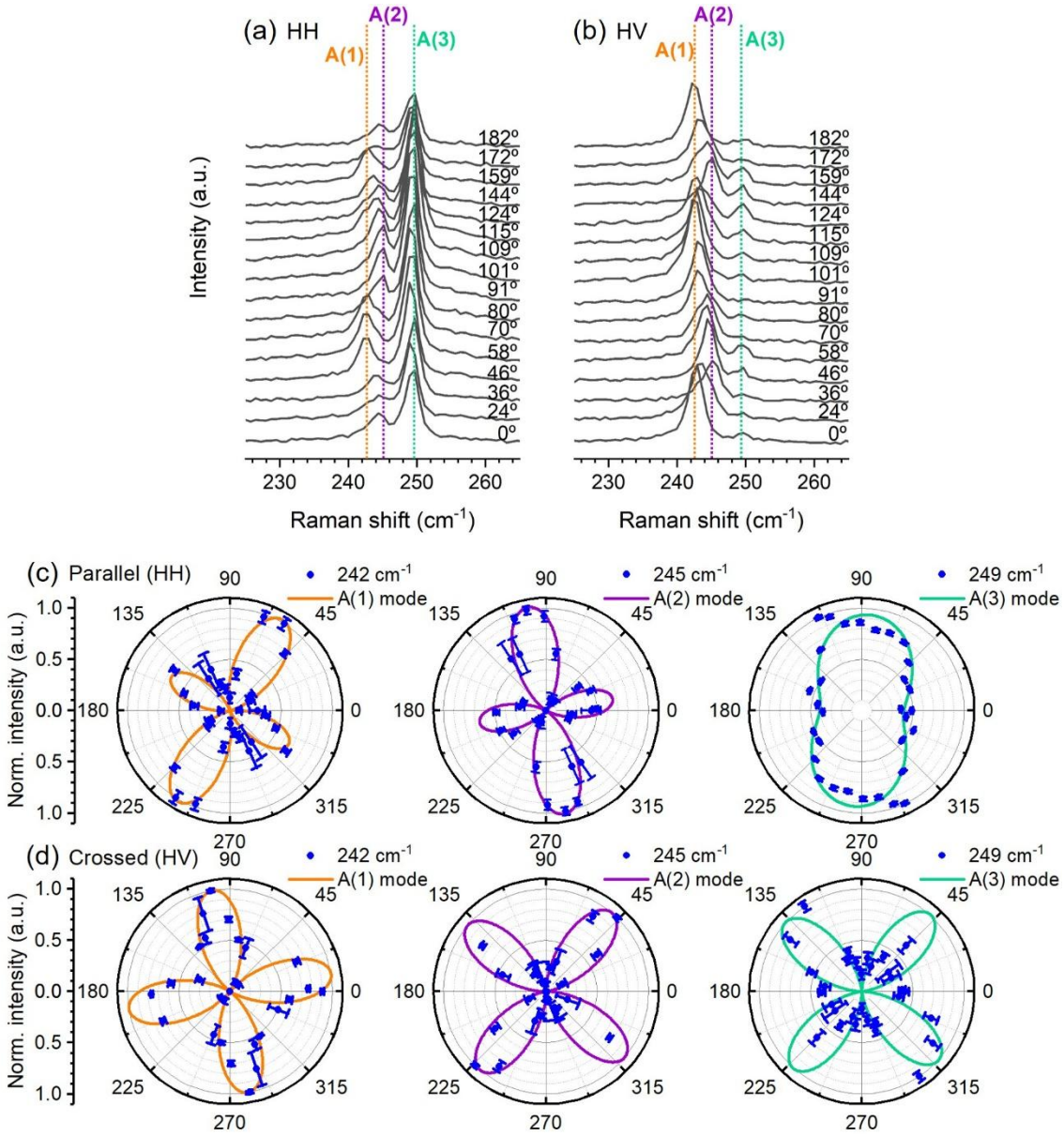

Figure 2. Polarization-resolved Raman response of uniaxially strained WSe_2 acquired with 457 nm excitation. (a,b) Angle-dependent Raman spectra acquired under parallel (HH) and crossed (HV) polarization configurations, respectively, during sample rotation under fixed uniaxial strain of 1.6%. (c,d) Polar plots of the two split in-plane modes and the out-of-plane mode acquired under parallel (HH) and crossed (HV) polarization configurations. Symbols represent the experimental Raman

intensities extracted from the angle-dependent Raman spectra shown in (a,b), with error bars corresponding to the fitting uncertainty. Solid lines are theoretical calculations based on the C_1 Raman tensors (see Supplementary Note 2). Dotted lines are used as guides to the eye to better visualize the the position of the Raman modes. Due to the reduced symmetry induced by uniaxial strain, the in-plane E mode splits into two components, A(1) (orange line) and A(2) (purple line), and the out-of-plane A1 becomes A(3) (green line).

Figures 2a and 2b show the angle-dependent Raman spectra acquired under HH and HV configurations, respectively. Under both polarization geometries, the relative intensities of the Raman modes evolve systematically with sample rotation, producing a pronounced angular dependence absent in the unstrained state (Supplementary Note 4). Most notably, under crossed polarization, the out-of-plane Raman contribution A(3) becomes visible, in contrast to its absence under unstrained conditions.

The Raman intensities extracted from the spectra are summarized in the polar plots shown in Figures 2c and 2d. Both the split in-plane modes and the out-of-plane contribution exhibit characteristic anisotropic modulation patterns that are accurately reproduced by calculations based on the C_1 Raman tensors (solid lines). In contrast, unstrained WSe_2 on Au exhibits the expected isotropic response associated with C_{3v} symmetry. [42]

Under uniaxial strain, the crystal symmetry is reduced from C_{3v} to C_s when the strain axis coincides with a mirror plane and to C_1 for a general strain direction. The angular dependence observed experimentally is consistent with the latter case, as the two in-plane modes are better described by a fourfold dependence with asymmetric lobes, as predicted by the C_1 point group, rather than the fourfold and twofold lobes expected by Cs symmetry. As discussed in Supplementary Note 2, symmetry lowering not only lifts the double degeneracy of the in-plane mode but also modifies the Raman tensors, giving rise to the observed polarization dependence.

These observations demonstrate that the Raman spectral evolution under uniaxial strain reflects more than simply the progressive spectral separation of overlapping phonon modes. Instead, the Raman response is governed by symmetry lowering and the associated modification of the Raman selection rules. As discussed in Supplementary Note 2, the reduction of the lattice symmetry from C_{3v} to C_1 not only lifts the double degeneracy of the

in-plane phonon mode but also modifies the Raman tensors, leading to the characteristic angular and polarization dependence observed experimentally. Consequently, the polarization response provides direct access to the symmetry of the applied deformation rather than simply to the evolution of the Raman frequencies. Importantly, even below the strain required to spectrally resolve the in-plane mode splitting, the appearance of finite Raman intensity under crossed polarization provides a reliable experimental fingerprint of uniaxial strain.

Polarization fingerprints of biaxial strain

We next investigate the Raman response of WSe_2 under biaxial strain. Figure 3a shows the evolution of the Raman spectra acquired under increasing biaxial deformation up to ~1.25% strain. Both the in-plane and out-of-plane Raman modes progressively shift with increasing strain, while no clear lifting of the in-plane mode degeneracy is observed. Because the in-plane mode shifts at a higher rate than the out-of-plane mode (see Supplementary Note 5), a well-defined double-peak structure progressively emerges, closely resembling the apparent splitting observed under uniaxial strain.

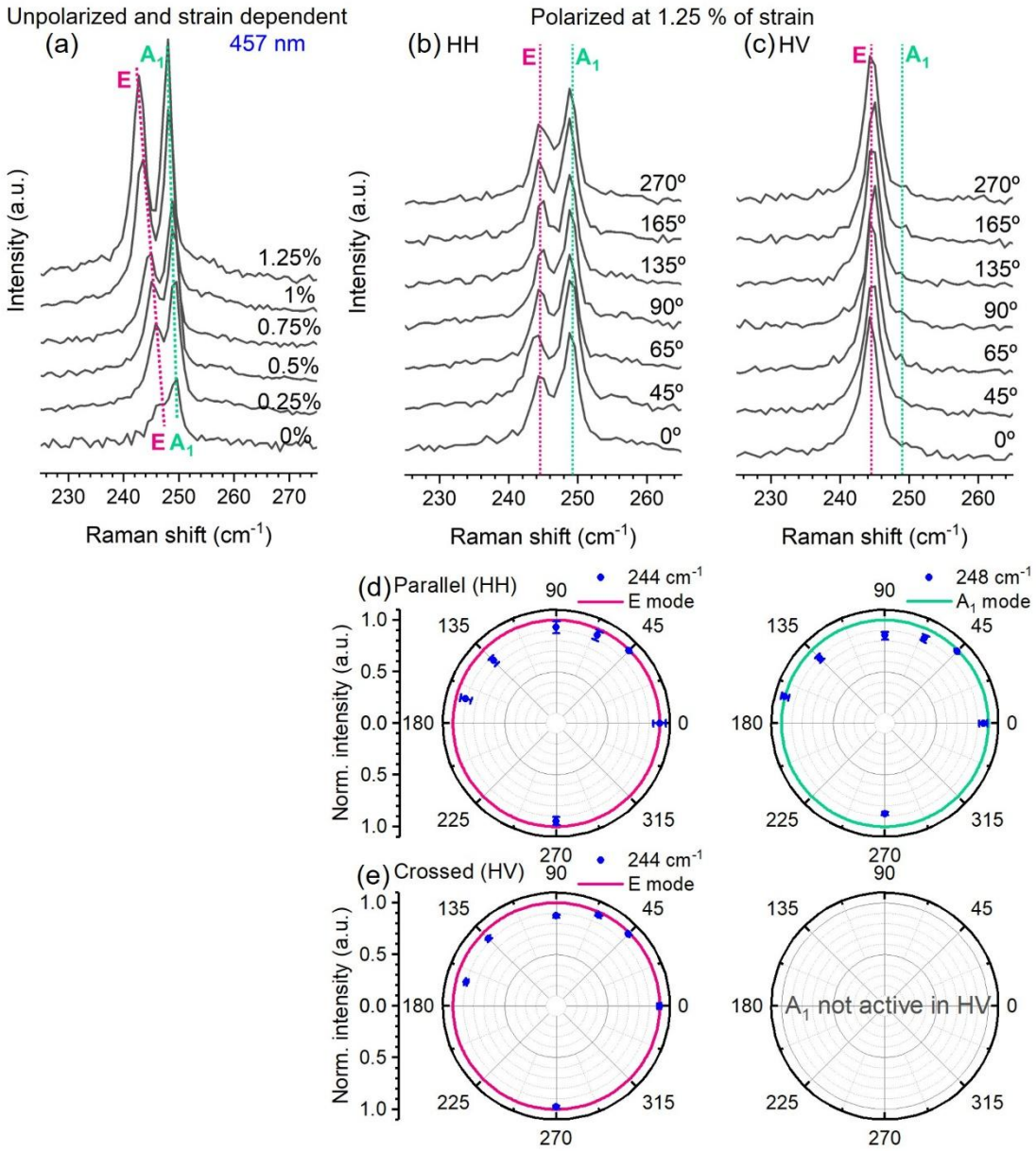

Figure 3. Raman response of biaxially strained WSe_2 acquired with 457 nm excitation. (a) Unpolarized Raman spectra acquired under increasing biaxial strain up to ~1.25%. (b,c) Angle-dependent Raman spectra acquired under parallel (HH) and crossed (HV) polarization configurations, respectively, during sample rotation under fixed biaxial strain of ~1.25%. (d,e) Polar plots of the in-plane and out-of-plane Raman modes acquired under parallel (HH) and crossed (HV) polarization configurations. Symbols represent the experimental Raman intensities extracted from the angle-dependent Raman spectra shown in (b,c), with error bars corresponding to the fitting uncertainty. Solid lines are theoretical calculations based on the C_{3v} Raman tensors (see Supplementary Note 2). Dotted lines are used as guides to the eye to better visualize the position of the Raman modes. Pink and green lines indicate the in-plane (E) and out-of-plane (A1) modes, respectively.

Figures 3b and 3c show the angle-dependent Raman spectra acquired under HH and HV configurations, respectively. In contrast to uniaxial strain, the spectra remain essentially unchanged upon sample rotation, indicating the absence of strain-induced angular anisotropy. In particular, the out-of-plane contribution remains inactive under crossed polarization at all measured angles.

The Raman intensities extracted from the spectra are summarized in the polar plots shown in Figures 3d and 3e. Both Raman modes exhibit nearly isotropic angular distributions that are accurately reproduced by calculations based on the C_{3v} Raman tensors (solid lines), confirming that the lattice symmetry is preserved under biaxial deformation. Under crossed polarization, the out-of-plane contribution remains inactive, consistent with preservation of the original Raman selection rules and the absence of symmetry lowering.

These observations demonstrate that the apparent spectral separation observed under biaxial strain arises from a fundamentally different physical mechanism than that observed under uniaxial deformation. Rather than reflecting symmetry lowering and lifting of the in-plane mode degeneracy, the spectral evolution originates from the different strain sensitivities of the overlapping E and A_1 phonons, while the lattice symmetry and Raman selection rules remain unchanged. Consequently, the polarization response remains rotationally invariant and the out-of-plane mode stays inactive under crossed polarization. Therefore, despite producing similar unpolarized Raman spectra, uniaxial and biaxial strain exhibit fundamentally different polarization fingerprints. Together with the uniaxial results, these measurements establish polarization-resolved Raman spectroscopy as a direct experimental route for distinguishing between uniaxial and biaxial strain in WSe_2.

Symmetry fingerprints of strain geometry in WSe_2

The polarization responses observed under uniaxial and biaxial strain establish direct symmetry fingerprints for identifying the geometry of the applied strain in WSe_2. Figure 4 summarizes the Raman fingerprints associated with both strain regimes. Under uniaxial deformation, strain applied along a single direction lowers the lattice symmetry from C_{3v} to C_1, producing an anisotropic Raman response, activation of the out-of-plane mode under crossed polarization, and lifting of the in-plane mode degeneracy. In contrast, biaxial strain

preserves the in-plane C_{3v} symmetry through isotropic lattice expansion, maintaining a rotationally invariant Raman response together with suppression of the out-of-plane contribution under crossed polarization (Figure 4b).

Although unpolarized Raman spectra may appear qualitatively similar under both strain regimes, polarization-resolved Raman measurements reveal fundamentally different symmetry fingerprints. Under biaxial strain, the Raman response remains rotationally invariant and the out-of-plane mode stays inactive in the HV configuration. In contrast, uniaxial strain produces pronounced angular anisotropy together with activation of the out-of-plane mode under crossed polarization, leading to distinct spectral responses at different rotation angles (Figure 4c). These complementary fingerprints establish polarization-resolved Raman spectroscopy as a simple and robust experimental approach for distinguishing uniaxial and biaxial strain in WSe_2.

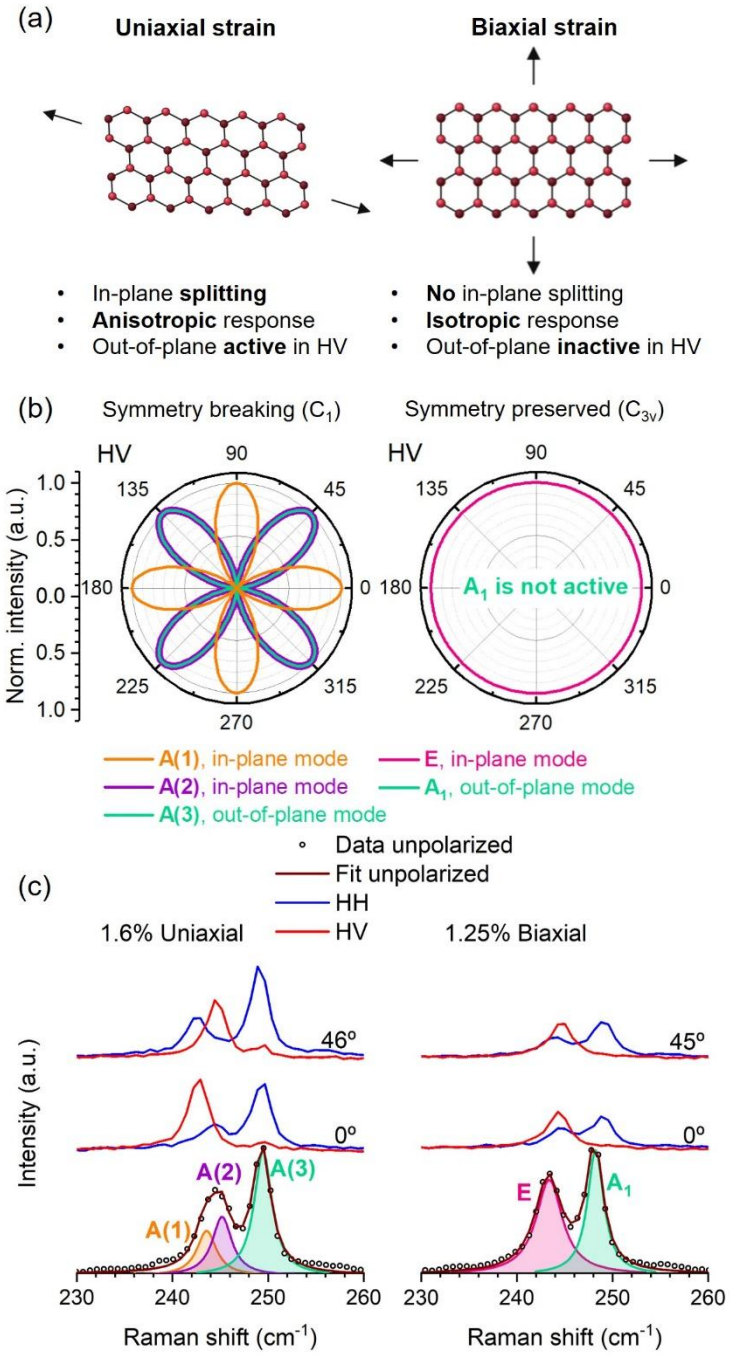

Figure 4. Conceptual symmetry fingerprints of uniaxial and biaxial strain in WSe_2. Schematic summary comparing the (a) lattice deformation, (b) crystal symmetry, and (c) polarization-resolved Raman fingerprints associated with uniaxial and biaxial strain in WSe_2. Under uniaxial strain, symmetry lowering from C_{3v} to C_1 lifts the degeneracy of the in-plane Raman mode and modifies the Raman tensors, giving rise to characteristic four-lobed angular intensity patterns, and activation of the out-of-plane mode under crossed (HV) polarization. In contrast, biaxial strain preserves the C_{3v} symmetry through isotropic lattice expansion. Consequently, the out-of-plane mode remains inactive in the HV configuration, while the in-plane mode exhibits rotationally invariant Raman intensity in both HH and HV configurations.

Overall, we demonstrate that polarization-resolved Raman spectroscopy provides direct symmetry fingerprints for distinguishing uniaxial and biaxial strain in WSe_2. Although both deformation regimes produce remarkably similar unpolarized Raman spectra, their polarization responses reveal fundamentally different symmetry changes and physical mechanisms. Under uniaxial strain, symmetry lowering lifts the degeneracy of the in-plane phonon mode and modifies the Raman selection rules, whereas biaxial strain preserves the lattice symmetry and produces similar spectral evolution through the different strain sensitivities of overlapping phonon modes. The large strain range experimentally accessible in our configuration further enables direct resolution of the splitting of the in-plane E mode under uniaxial strain.

Beyond resolving the ambiguity associated with the congested E/A_1 spectral region of WSe_2, this work demonstrates that the angular and polarization dependence of the Raman response provides direct experimental access to the symmetry of the applied deformation. The comparison between 532 and 457 nm excitation further highlights the importance of selecting appropriate excitation conditions for reliable symmetry analysis. More broadly, these results establish polarization-resolved Raman spectroscopy as a robust and experimentally accessible approach for identifying strain symmetry in two-dimensional materials with complex or spatially inhomogeneous strain fields, where the key information is contained not only in the Raman frequencies themselves, but also in their symmetry-dependent polarization response.

Methods

Sample preparation

WSe_2 (HQ Graphene) was mechanically exfoliated using Au-assisted exfoliation onto flexible polycarbonate (PC) substrates (250 μm thick) suitable for strain engineering. The PC substrates were coated with 3 nm Ti and 6 nm Au using a home-built electron-beam evaporator. Mono-, bi- and trilayer regions were identified through optical microscopy and Raman spectroscopy.

Strain setups

Uniaxial strain was applied using a motorized three-point bending platform. This setup enables the application of controlled tensile strain. Strain calibration was performed using lithographically patterned micropillar arrays providing a direct assessment of the applied deformation. Biaxial strain was applied using a home-built cruciform bending stage. Strain calibration was also performed using the micropillars. Further details of the strain setup calibration method and analysis are presented below and in previous works.[39,41]

Uniaxial strain: Uniaxial strain was applied using the automated straining setup previously developed and experimentally calibrated in Ref.[41]. In a three-point bending setup, the strain (ε) at the substrate surface is given by:

$$\varepsilon = \frac{6Dt}{L^2} \quad (1)$$

where D is the substrate deflection, t is the substrate thickness, and L is the distance between the supporting points. Previously [41], this geometrical relation was experimentally validated using lithographically patterned photoresist micropillar arrays on the surface of identical flexible substrates. The strain was independently determined from the relative change in pillar separation according to:

$$\varepsilon = \frac{l - l_0}{l_0} \quad (2)$$

where l and l_0 are the pillar separations at a given and zero substrate deflection, respectively. The experimentally measured strain values were in good agreement with those calculated from the three-point-bending geometry. From the experimental uncertainty of the micropillar calibration, we estimate the uncertainty in the applied strain to be approximately ±0.15% across the entire strain range investigated.[41]

Strain was applied using a motorized translation stage based on the previously reported setup [40], providing highly accurate displacement control (5 μm deviation for a target displacement of 1 mm). We note that this calibration determines the nominal strain at the substrate surface. The actual strain experienced by the supported 2D material additionally

depends on the strain-transfer efficiency at the 2D material/substrate interface. This aspect is particularly relevant for the present Au-assisted configuration. In our previous work using the same gold-assisted exfoliation approach on flexible PC substrates [35], we demonstrated that the presence of the Au interfacial layer substantially improves strain transfer to the supported 2D material and mitigates slippage compared with flakes directly supported on PC. This enhanced mechanical coupling was attributed to the strong interaction between the 2D material and Au and allowed uniaxial strains as high as 3% to be transferred to trilayer MoS_2 before the onset of slippage. Therefore, the maximum uniaxial strain of 2.5% employed here lies within the range previously demonstrated to be accessible using this Au-assisted configuration.

Biaxial strain: Biaxial strain was applied using the bending/indentation of a cruciform polycarbonate substrate described in [39], where the construction and calibration of the platform are provided in detail. The strain calibration was experimentally performed using lithographically patterned micropillar arrays on equivalent cruciform substrates. Rather than relying on the continuum mechanics model that relates the vertical displacement of the cruciform to the biaxial strain at its center, the applied strain was directly determined from the relative change in the distance between the micropillars using Equation 2.

The experimentally determined biaxial strain varies linearly with the vertical displacement (Z) of the translation stage, $\varepsilon = kZ$, with a calibration factor of approximately 2.3%/mm [36]. This experimental calibration was used to convert the actuator displacement into the biaxial strain values reported throughout the manuscript. The estimated uncertainty associated with the biaxial strain values is ± 0.15%, according to Ref. [36].

Importantly, the homogeneity and reversibility of the biaxial deformation generated by this platform were already experimentally assessed in Ref. [36]. Spatially resolved measurements showed a homogeneous strain response over the relevant region of the cruciform substrate, while repeated loading–unloading cycles demonstrated the reproducibility and reversibility of the applied deformation. In addition, polarization-resolved Raman measurements of WSe_2 showed that the A_1 mode remains inactive in crossed polarization upon strain application, indicating preservation of the relevant crystal symmetry and supporting the biaxial character of the applied deformation.

Raman spectroscopy

Raman measurements were performed using a confocal Raman microscope, MonoVista CRS+ system (Spectroscopy and Imaging GmbH), equipped with 457 nm and 532 nm excitation lasers. A 50× objective and a 2400 lines/mm diffraction grating were used for all the measurements. Laser power was kept below 0.5 mW to avoid heating the flakes. The spectra were collected with a 60 s integration time. Polarization-resolved measurements were carried out under parallel (HH) and crossed (HV) configurations, with a polarization leakage estimated to be below 2%. Angular-dependent measurements were performed by rotating the straining stage together with the mounted sample while maintaining the polarization of the incident and scattered light fixed (either parallel or crossed). Spectral fitting was performed using Lorentzian functions (see Supplementary Note 4).

Data Availability

The raw data supporting the findings of this study have been deposited in the Zenodo open repository and are available at https://doi.org/10.5281/zenodo.22819683. Additional information is available from the corresponding author upon request.

Competing Interests

Author A. C.-G. is an Editorial Board member of npj 2D Materials and Applications. A. C.-G. was not involved in the journal's review of, or decisions related to, this manuscript. The other authors declare no competing financial or non-financial interests.

Acknowledgements

ICMM-CSIC authors acknowledge support from the Severo Ochoa Centres of Excellence program and the IFIMAC authors acknowledge support from the Maria de Maeztu program for Units of Excellence in R&D.

Funding

A.R. acknowledges funding from the European Union under the Marie Skłodowska-Curie (GA 101109987). M.M.G., A.R. and P.A. acknowledge funding from the European Research Council (ERC) through the ERC StG HeaT2Defects project (GA 101163902). P.A. acknowledges support from Grants PID2022-142331NB-I00 and CNS2023-143713, funded by MICIU/AEI/10.13039/501100011033. P.A. also acknowledges the "Comunidad de Madrid" for the financial support to the CMOFs4water-CM Project (TEC-2024/ECO-332) through the R&D activities programme "Tecnologías 2024". A.C.-G. and C.M. acknowledge support from Grant PID2023-151946OB-I00, funded by MICIU/AEI/10.13039/501100011033 and by ERDF/EU. A.C.-G. also acknowledge funding from the European Research Council (ERC) through the ERC-2024 SyG SKIN2DTRONICS project (GA 101167218). ICMM-CSIC authors acknowledge support from the Severo Ochoa Centres of Excellence program through Grant CEX2024-001445-S, and the IFIMAC authors acknowledge support from the Maria de Maeztu program for Units of Excellence in R&D through Grant CEX2023-001316-M, both programs funded by MICIU/AEI/10.13039/501100011033.

References

[1] Roldán R, Castellanos-Gomez A, Cappelluti E and Guinea F Strain engineering in semiconducting two-dimensional crystals *J. Phys. Condens. Matter* **27** 313201 (2015)

[2] Peng Z, Chen X, Fan Y, Srolovitz D J and Lei D Strain engineering of 2D semiconductors and graphene: from strain fields to band-structure tuning and photonic applications *Light Sci. Appl.* **9** 190 (2020)

[3] Blundo E, Cappelluti E, Felici M, Pettinari G and Polimeni A Strain-tuning of the electronic, optical, and vibrational properties of two-dimensional crystals *Appl. Phys. Rev.* **8** 21318 (2021)

[4] Saito R, Tatsumi Y, Huang S, Ling X and Dresselhaus M S Raman spectroscopy of

transition metal dichalcogenides *J. Phys. Condens. Matter* **28** 353002 (2016)

[5] Mueller N S, Heeg S, Alvarez M P, Kusch P, Wasserroth S, Clark N, Schedin F, Parthenios J, Papagelis K, Galiotis C, Kalbáč M, Vijayaraghavan A, Huebner U, Gorbachev R, Frank O and Reich S Evaluating arbitrary strain configurations and doping in graphene with Raman spectroscopy *2D Mater.* **5** 15016 (2018)

[6] Schmidt R, Niehues I, Schneider R, Drüppel M, Deilmann T, Rohlfing M, de Vasconcellos S M, Castellanos-Gomez A and Bratschitsch R Reversible uniaxial strain tuning in atomically thin WSe 2 *2D Mater.* **3** 021011 (2016)

[7] Hernández López P, Heeg S, Schattauer C, Kovalchuk S, Kumar A, Bock D J, Kirchhof J N, Höfer B, Greben K, Yagodkin D, Linhart L, Libisch F and Bolotin K I Strain control of hybridization between dark and localized excitons in a 2D semiconductor *Nat. Commun.* **13** 7691 (2022)

[8] Aslan B, Deng M, Brongersma M L and Heinz T F Strained bilayer WSe2 with reduced exciton-phonon coupling *Phys. Rev. B* **101** 115305 (2020)

[9] Aslan B, Deng M and Heinz T F Strain tuning of excitons in monolayer WSe2 *Phys. Rev. B* **98** 115308 (2018)

[10] Lee J-U, Woo S, Park J, Park H C, Son Y-W and Cheong H Strain-shear coupling in bilayer MoS2 *Nat. Commun.* **8** 1370 (2017)

[11] Doratotaj D, Simpson J R and Yan J-A Probing the uniaxial strains in MoS2using polarized Raman spectroscopy: A first-principles study *Phys. Rev. B* **93** 075401 (2016)

[12] Hsu W-T, Lu L-S, Wang D, Huang J-K, Li M-Y, Chang T-R, Chou Y-C, Juang Z-Y, Jeng H-T, Li L-J and Chang W-H Evidence of indirect gap in monolayer WSe2 *Nat. Commun.* **8** 929 (2017)

[13] del Corro E, Terrones H, Elias A, Fantini C, Feng S, Nguyen M A, Mallouk T E, Terrones M and Pimenta M A Excited Excitonic States in 1L, 2L, 3L, and Bulk WSe2 Observed by Resonant Raman Spectroscopy *ACS Nano* **8** 9629–35 (2014)

[14] Terrones H, Corro E Del, Feng S, Poumirol J M, Rhodes D, Smirnov D, Pradhan N R, Lin Z, Nguyen M A T, Elías A L, Mallouk T E, Balicas L, Pimenta M A and

Terrones M New First Order Raman-active Modes in Few Layered Transition Metal Dichalcogenides *Sci. Rep.* **4** 4215 (2014)

[15] Dadgar A M, Scullion D, Kang K, Esposito D, Yang E H, Herman I P, Pimenta M A, Santos E-J G and Pasupathy A N Strain Engineering and Raman Spectroscopy of Monolayer Transition Metal Dichalcogenides *Chem. Mater.* **30** 5148–55 (2018)

[16] Kim S, Kim K, Lee J-U and Cheong H Excitonic resonance effects and Davydov splitting in circularly polarized Raman spectra of few-layer WSe2 *2D Mater.* **4** 45002 (2017)

[17] Blaga C, Labordet Álvarez Á, Balgarkashi A, Banerjee M, Fontcuberta i Morral A and Dimitrievska M Unveiling the complex phonon nature and phonon cascades in 1L to 5L WSe2 using multiwavelength excitation Raman scattering *Nanoscale Adv.* **6** 4591–603 (2024)

[18] del Corro E, Botello-Méndez A, Gillet Y, Elias A L, Terrones H, Feng S, Fantini C, Rhodes D, Pradhan N, Balicas L, Gonze X, Charlier J-C, Terrones M and Pimenta M A Atypical Exciton–Phonon Interactions in WS2 and WSe2 Monolayers Revealed by Resonance Raman Spectroscopy *Nano Lett.* **16** 2363–8 (2016)

[19] Luo X, Zhao Y, Zhang J, Toh M, Kloc C, Xiong Q and Quek S Y Effects of lower symmetry and dimensionality on Raman spectra in two-dimensional WSe2 *Phys. Rev. B* **88** 195313 (2013)

[20] Desai S B, Seol G, Kang J S, Fang H, Battaglia C, Kapadia R, Ager J W, Guo J and Javey A Strain-Induced Indirect to Direct Bandgap Transition in Multilayer WSe2 *Nano Lett.* **14** 4592–7 (2014)

[21] Sahin H, Tongay S, Horzum S, Fan W, Zhou J, Li J, Wu J and Peeters F M Anomalous Raman spectra and thickness-dependent electronic properties of WSe2 *Phys. Rev. B* **87** 165409 (2013)

[22] Michail A, Yang J A, Filintoglou K, Balakeras N, Nattoo C A, Bailey C S, Daus A, Parthenios J, Pop E and Papagelis K Biaxial Strain Transfer in Monolayer MoS2 and WSe2 Transistor Structures *ACS Appl. Mater. Interfaces* **16** 49602–11(2024)

[23] Yang J A, Bennett R K A, Hoang L, Zhang Z, Thompson K J, Michail A, Parthenios

J, Papagelis K, Mannix A J and Pop E Biaxial Tensile Strain Enhances Electron Mobility of Monolayer Transition Metal Dichalcogenides *ACS Nano* **18** 18151–9 (2024)

[24] Kourmoulakis G, Michail A, Paradisanos I, Marie X, Glazov M M, Jorissen B, Covaci L, Stratakis E, Papagelis K, Parthenios J and Kioseoglou G Biaxial strain tuning of exciton energy and polarization in monolayer WS2 *Appl. Phys. Lett.* **123** 223103 (2023)

[25] Smiri B, Meyer T, LE V-H, Cadot S, Gauthier N, Jamil R, Mazel Y, Deschanvres J L, Pelissier B and Nolot E Layer-dependent Raman polarization anisotropy in MoS_2 films grown by 200 mm-scale atomic layer deposition *Sci. Rep.* **16** 2187 (2026)

[26] Hu B, Xie X, Ouyang X, Chen J, Li S, He J, Liu Z, Wang J-T and Liu Y Unveiling optical anisotropy in disrupted symmetry WSe2/SiP heterostructures *Nano Res.* **17** 8585–91 (2024)

[27] Chen S-Y, Zheng C, Fuhrer M S and Yan J Helicity-Resolved Raman Scattering of MoS2, MoSe2, WS2, and WSe2 Atomic Layers *Nano Lett.* **15** 2526–32 (2015)

[28] Kim J, Lee J-U and Cheong H Polarized Raman spectroscopy for studying two-dimensional materials *J. Phys. Condens. Matter* **32** 343001 (2020)

[29] Ma X, Guo P, Yi C, Yu Q, Zhang A, Ji J, Tian Y, Jin F, Wang Y, Liu K, Xia T, Shi Y and Zhang Q Raman scattering in the transition-metal dichalcogenides of 1T′-MoT e2,Td-MoT e2, and Td-WT e2 *Phys. Rev. B* **94** 214105 (2016)

[30] Quan J, Chen G, Linhart L, Liu Z, Taniguchi T, Watanabe K, Libisch F, Huang R and Li X Quantifying Strain in Moiré Superlattice *Nano Lett.* **23** 11510–6 (2023)

[31] Rodríguez Á, Varillas J, Haider G, Kalbáč M and Frank O Complex Strain Scapes in Reconstructed Transition-Metal Dichalcogenide Moiré Superlattices *ACS Nano* **17** 7787–96 (2023)

[32] Zhu W, Liang L, Roberts R H, Lin J and Akinwande D Anisotropic Electron–Phonon Interactions in Angle-Resolved Raman Study of Strained Black Phosphorus *ACS Nano* **12** 12512–22 (2018)

[33] Blundo E, Surrente A, Spirito D, Pettinari G, Yildirim T, Chavarin C A, Baldassarre

L, Felici M and Polimeni A Vibrational Properties in Highly Strained Hexagonal Boron Nitride Bubbles *Nano Lett.* **22** 1525–33 (2022)

[34] Roy S, Gao J and Yang X Upconversion photoluminescence of monolayer WSe2 with biaxial strain tuning *Opt. Express* **32** 3308 (2024)

[35] Rodríguez Á, Çakıroğlu O, Li H, Carrascoso F, Mompean F, Garcia-Hernandez M, Munuera C and Castellanos-Gomez A Improved Strain Transfer Efficiency in Large-Area Two-Dimensional MoS2 Obtained by Gold-Assisted Exfoliation *J. Phys. Chem. Lett.* **15** 6355–62 (2024)

[36] Rodríguez Á, Munuera C and Castellanos-Gomez A Mechanical Detuning of Exciton–Phonon Resonance in WS2 *ACS Photonics* **13** 2199–205 (2026)

[37] Panasci S E, Schilirò E, Roccaforte F and Giannazzo F Gold-Assisted Exfoliation of Large-Area Monolayer Transition Metal Dichalcogenides: From Interface Properties to Device Applications *Adv. Funct. Mater.* **35** 2414532 (2025)

[38] Velický M, Donnelly G E, Hendren W R, McFarland S, Scullion D, DeBenedetti W J I, Correa G C, Han Y, Wain A J, Hines M A, Muller D A, Novoselov K S, Abruña H D, Bowman R M, Santos E J G and Huang F Mechanism of Gold-Assisted Exfoliation of Centimeter-Sized Transition-Metal Dichalcogenide Monolayers *ACS Nano* **12** 10463–72 (2018)

[39] Carrascoso F, Frisenda R and Castellanos-Gomez A Biaxial versus uniaxial strain tuning of single-layer MoS2 *Nano Mater. Sci.* **4** 44–51 (2022)

[40] Çakıroğlu O, Island J O, Xie Y, Frisenda R and Castellanos-Gomez A An Automated System for Strain Engineering and Straintronics of 2D Materials *Adv. Mater. Technol.* **8** 2201091 (2023)

[41] Carrascoso F, Li H, Frisenda R and Castellanos-Gomez A Strain engineering in single-, bi- and tri-layer MoS2, MoSe2, WS2 and WSe2 *Nano Res.* **14** 1698–703 (2021)

[42] Rodriguez A, Velický M, Ř áhová J, Zólyomi V, Koltai J, Kalbáč M and Frank O Activation of Raman modes in monolayer transition metal dichalcogenides through strong interaction with gold *Phys. Rev. B* **105** 195413 (2022)

[43] Conley H J, Wang B, Ziegler J I, Haglund R F J, Pantelides S T and Bolotin K I Bandgap Engineering of Strained Monolayer and Bilayer MoS2 *Nano Lett.* **13** 3626–30 (2013)

[44] Zhu C R, Wang G, Liu B L, Marie X, Qiao X F, Zhang X, Wu X X, Fan H, Tan P H, Amand T and Urbaszek B Strain tuning of optical emission energy and polarization in monolayer and bilayer MoS2 *Phys. Rev. B* **88** 121301 (2013)

[45] Vandalon V, Sharma A, Perrotta A, Schrode B, Verheijen M A and Bol A A Polarized Raman spectroscopy to elucidate the texture of synthesized MoS2 *Nanoscale* **11** 22860–70 (2019)

[46] Li H, Sanchez-Santolino G, Puebla S, Frisenda R, Al-Enizi A M, Nafady A, D'Agosta R and Castellanos-Gomez A Strongly Anisotropic Strain-Tunability of Excitons in Exfoliated ZrSe3 *Adv. Mater.* **34** 2103571 (2022)

Supplementary Files

This is a list of supplementary files associated with this preprint. Click to download.

- SymmetryresolvedRamanfingerprintsofuniaxialandbiaxialstrainin WSe...SIv1clean.pdf